UNIVERSITY OF TARTU
FACULTY OF SCIENCE AND TECHNOLOGY
Institute of Chemistry
Chair of Physical Chemistry

Joel Indrek Martin Laanemäe

Fe-N/C Catalysts Based on Carbon Derived from Waste Tires: Advancing Oxygen Reduction Reaction in Alkaline Solution

Master's thesis (30 ECTS)

Materials Science and Technology

Supervisor: Rutha Jäger, PhD

Tartu 2024

Fe-N/C Catalysts Based on Carbon Derived from Waste Tires: Advancing Oxygen Reduction Reaction in Alkaline Solution

Nine Fe-N/C catalysts were synthesized using carbon derived from waste tire granules (C1 or C2, whereby C2 contained fewer elemental impurities and a lower specific surface area), Fe salt, N compound (guanidine carbonate or dicyandiamide), and pore formers ($ZnCl_2$ and/or hydroxyapatite) at different pyrolysis temperatures (800, 900 or 1000 °C). Physical characterization included HR-SEM, SEM-EDX, N_2 sorption, and XRD analyses. The rotating disk electrode (RDE) method was used to estimate the catalysts' activity toward the oxygen reduction reaction (ORR) in 0.1 M KOH solution. All catalysts exhibited higher ORR activity compared to the carbon precursors. It was concluded that the choice of synthesis parameters has a major impact on the catalysts' physical characteristics and ORR activity. The most active ORR catalyst exhibited a very good onset potential value (E_{onset} = 0.92 V vs RHE).

Keywords: Fe-N/C catalyst, ORR, waste tire derived carbon, RDE method.
CERCS classification: T140 Energy research, P401 Electrochemistry

Fe-N/C katalüsaatorid kasutades rehvipurust sünteesitud süsinikku: hapniku redutseerumisreaktsioon leeliselises lahuses

Töö käigus sünteesiti üheksa Fe-N/C katalüsaatorit kasutades rehvipurust sünteesitud süsinikmaterjali (C1 või C2, seejuures C2 sisaldas vähem lisandeid ja oli väiksema eripinnaga), Fe-soola, N-ühendit (guanidiinkarbonaat või ditsüaandiamiid) ja poorimoodustajat ($ZnCl_2$ ning kahe materjali puhul ka hüdroksüapatiiti) erinevatel pürolüüsitemperatuuridel (800, 900 või 1000 °C). Materjale uuriti HR-SEM, SEM-EDX, N_2 sorptsioon ja XRD meetoditega. Pöörleva ketaselektroodi (RDE) meetodit kasutati materjalide hapniku redutseerumisreaktsiooni (ORR) aktiivsuse määramiseks 0.1 M KOH lahuses. Kõik Fe-N/C katalüsaatorid olid ORR suhtes aktiivsemad kui modifitseerimata süsinikmaterjalid. Leiti, et sünteesiparameetrid mõjutavad oluliselt saadud katalüsaatorite füüsikalisi ja elektrokeemilisi omadusi. Kõige aktiivsemal ORR katalüsaatormaterjalil oli väga hea lainealgus-potenstiaali väärtus (E_{onset} = 0.92 V vs RHE).

Märksõnad: Fe-N/C katalüsaator, hapniku redutseerumine, pöörleva ketaselektroodi meetod.
CERCS classification: T140 Energeetika, P401 Elektrokeemia

Table of Contents

Introduction

In the past few years, the Intergovernmental Panel on Climate Change (IPCC) has published multiple reports on the human contribution to climate change [1]. Their grim predictions of even the best-case scenarios for the foreseeable future provided an alarming wake-up call – even though it has long been understood that fossil fuels in the energy and transportation sector are responsible for a large fraction of carbon emissions.

One alternative energy system in the transportation sector and industry is the implementation of hydrogen technologies. Electrolyzers produce hydrogen using surplus green energy and fuel cells consume hydrogen to generate electrical energy. In recent years, copious large-scale hydrogen energy projects have been initiated. While the EU and the US have planned large sums to fund large hydrogen projects, some Asian regions are well ahead in terms of realizing large-scale projects. For example, South Korea's Hyundai produced over ten thousand hydrogen-powered cars, the NEXO, in 2022 and Toyota shipped around 4000 of their fuel cell electric vehicles, the Mirai. These cars use the proton exchange membrane fuel cell (PEMFC) which remains the most produced type of fuel cell. [2] While efficient, they rely on expensive platinum-containing catalysts [3–7]. The necessity of catalysts in the first place comes from the fact that the reaction on the cathode of a PEMFC, the oxygen reduction reaction (ORR), is sluggish without a catalyst [8]. Researchers have put ample effort into developing less expensive, yet efficient catalysts for fuel cells. This might involve using less platinum in the catalyst or replacing platinum altogether.

Non-platinum group metal (NPGM) catalysts, such as iron and nitrogen doped carbon materials (Fe-N/C), are a strong alternative to platinum-based catalysts – especially in alkaline media –, and are therefore used in alkaline exchange membrane fuel cells (AEMFC) [3,5,7]. Their main advantage is their low cost – Fe-N/C catalysts are much cheaper than Pt-containing catalysts. The electrochemical properties of an Fe-N/C catalyst rely on the choice of Fe and N precursors as well as the choice of carbon material [9–13]. One potential carbon source for such catalysts is waste tires. While 97% of end-of-life tires were recovered in the EU in 2021 [14], they have limited applications when it comes to reuse and recycling [15]. Of all the tires recovered in the EU, 42% were burnt for energy use and only half of the remaining material was recycled [14]. Another common tire disposal strategy outside of the EU is to store waste tires in landfills, which takes up land and poses environmental risks [16,17]. Neither burning waste tires nor their storage in landfills is particularly environmentally friendly. Producing carbon materials for fuel cell catalysts could provide a reasonable second life to waste tires.

This work aimed to develop Fe-N/C catalyst materials using waste tire derived carbon for efficient oxygen reduction reaction in an alkaline solution. Nine Fe-N/C catalysts were synthesized by varying several parameters: using two different nitrogen precursors, two different carbon materials, different nitrogen precursor amounts, adding an additional pore former, and varying the pyrolysis temperature. The study aimed to evaluate the impact of these synthesis parameters on the electrochemical and physical properties of the catalysts. To evaluate electrochemical activity, the rotating disk electrode method was used in an alkaline solution. HR-SEM was used to evaluate the materials' surface characteristics, SEM-EDX provided information on their elemental composition, nitrogen sorption gave insight into their pore characteristics, and XRD was used to further study the chemical composition of some catalyst materials.

1. Literature overview

1.1. AEMFC

Fuel cells are used to generate electric current from hydrogen. Various fuel cell types exist for different applications, including portable auxiliary power units, stationary power generation units, and vehicles. The most popular type of fuel cell for vehicles is the proton exchange membrane fuel cell (PEMFC). The PEMFC is used in hydrogen-powered cars, which are produced in the tens of thousands per year [2]. The PEMFC inherently has a strongly corrosive acidic medium [18], which means that the materials used in the PEMFC must be very resistant to corrosion. This substantially increases the fuel cell's cost. First, the types of catalysts that can be used are limited – usually expensive Pt-group metal catalysts are chosen for their corrosion resistance [4,19] and because they enable the adsorption of O_2 at an optimal binding energy [3]. Platinum is also scarce [5,20], which limits the total number of hydrogen-powered vehicles that could be built with PEMFC technology [21], and human labor conditions in platinum mines are poor [22]. Secondly, the membrane of the PEMFC is typically made from perfluorinated ionomers, which are produced using toxic HF and are neither environmentally friendly nor simple to produce [23]. Additionally, bipolar plates – another important component of PEMFCs – are coated with expensive materials and are complex to manufacture [5].

The anion exchange membrane fuel cell (AEMFC) can be used in similar applications as the PEMFC. However, it works in an alkaline environment, which enables the use of a wider range of more cost-effective catalysts, such as non-platinum group metal (NPGM) catalysts [4,6,18]. The AEMFC can apply cheaper and more easily manufactured bipolar plates and hydrocarbon-based ionomers. Still, AEMFC research has gained momentum much later than PEMFC research, which means that well-working industry standards for membranes or other components have yet to be established. [5]

The AEMFC (Figure 1) consists of an anode and a cathode, separated by an anion exchange membrane (AEM). The AEM is an electric insulator but an OH^- conductor. On the anode, hydrogen gas is adsorbed and oxidized, and as a result, electrons are generated. On the cathode, the oxygen is adsorbed and reduced (oxygen reduction reaction – ORR) and OH^- anions are formed. The OH^- anions migrate through the AEM to participate as a reactant in the anode reaction. As a result, an electric current is created between the anode and cathode. [24]

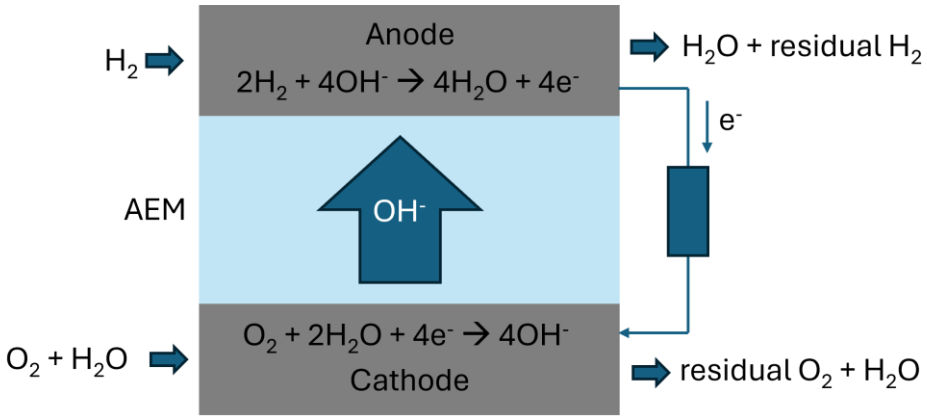

Figure 1. *Simplified working principle of an alkaline exchange membrane fuel cell.*

The AEMFC faces a similar problem as other fuel cell and battery technologies: the kinetics of the oxygen reduction reaction at the cathode are slow [8,25]. While this process is more favorable in alkaline media compared to acidic media, it is still the limiting process of the whole fuel cell, even in the AEMFC [26]. This is why catalyst research plays an integral role in the development of fuel cell technology.

1.2. Carbon materials

Porous carbon materials are well suited as support material for different kinds of catalysts for the ORR because of their chemical and mechanical stability, surface characteristics, and graphitic structure [7]. Their relatively large surface area (typically hundreds to a few thousand $m^2\ g^{-1}$) allows for a large number of active sites to form during catalyst synthesis. For the ORR to take place, it is crucial that the catalyst's active sites are accessible to O_2 and H_2O species, and that electrons have a low-resistance path away from the active site. The porous nature of carbons allows for O_2 and H_2O migration, and graphitic structures work well as electron conductors [5].

Cabon materials suited for fuel cell catalyst supports could be synthesized from any raw material that contains carbon, whereby the physical and electrochemical properties of the resulting carbon material vary a lot depending on the carbon source used. Researchers are more and more interested in using biological sources (such as coconut husks [13], lignin [9], peat [11,12] or coffee grounds [10]) as carbon feedstocks because of their abundant supply, exceptionally low cost, and high carbon content.

Another source of carbon is waste tires, as they contain around 20–35% carbon black and 45–65% natural and synthetic rubbers. Carbon black is mainly used to strengthen the tire rubber. The rest of a tire's mass consists of filler materials (such as clay or silica) and residual elements

from the vulcanization process of rubber (mainly Zn and S). The carbon black can be recovered through pyrolysis. During heat treatment, some of the rubber is carbonized, contributing to the carbon content of the resulting material. After pyrolysis, the solid fraction yield or char, mostly composed of carbon and ash, is around 40%, while the rest is a volatile fraction of gases and pyrolysis oil composed of a complex mixture of aliphatic and aromatic compounds. [15,27]

For AEMFC applications, the carbon must be modified with metal-containing or/and non-metallic compounds to achieve an efficient catalyst with high ORR activity.

1.3. Non-platinum group metal catalysts

The main benefit of the AEMFC is the possibility to use less expensive components due to its less corrosive alkaline medium. Hyun and Kim demonstrate that NPGM catalysts are two to five *orders of magnitude* less expensive than Pt catalysts. Furthermore, NPGM catalysts have shown better ORR activities compared to Pt in the AEMFC single cell. [3,5,7]

Various metal salts and nitrogen compound combinations can be used in the synthesis of NPGM catalysts. The choice of precursors and their ratios have a big impact on the catalyst's ORR activity. Fe, Co, Ni, and Cu have been studied extensively for NPGM catalysts, and Fe has been found to produce the most electrochemically active catalysts. Ligands that provide N_4 as the chelating atoms have been shown to create the most electrochemically active reaction centers. Additionally, macrocyclic transition metal compounds readily and irreversibly adsorb onto graphitic structures as catalyst sites, which makes such catalysts simple to synthesize. [8] It is debated whether metal atoms directly act as parts of the active sites for the ORR or whether they only catalyze the formation of active sites. Nonetheless, it is generally accepted that nitrogen dopants in carbon structures considerably improve ORR activity compared to carbon alone. [28]

Typically, a Fe-N/C type catalyst is made by heat treatment of a mixture of porous carbon, an iron source, and a nitrogen compound. Reaction centers are formed on the porous carbon's surface, where the ORR will take place [26]. Optimizing the porosity of a catalyst is important to achieve the best ORR activity: high microporosity facilitates the adsorption of O_2 while mesoporosity provides better oxygen mass transport [29,30]. Adding pore formers like $ZnCl_2$ has been proven to increase microporosity in carbon-based NPGM catalysts [29]. Secondly, hard templating with hydroxyapatite [30] or silica spheres [31] increases the mesoporosity of catalysts. Hydroxyapatite particles can take a needle-like shape with a diameter similar to the mesoporous range and therefore leave mesopores behind in the catalyst's structure. Another

benefit of hydroxyapatite is that it can be removed using milder acids, such as HNO_3, whereas silica is commonly removed using HF, which poses health risks and environmental hazards. [30] Alkaline treatment with KOH [29] or acid treatment with HNO_3 [32], and ball-milling [33] are also used to increase porosity. Higher pyrolysis temperatures are also known to increase the ORR activity of catalysts [30,34]. Therefore, a specific combination of precursors and synthesis parameters must be found to achieve the best possible results.

Although many studies have focused on the pyrolysis of waste tires [15,27,35–38] there is not a lot of research on the modification of pyrolyzed waste tire granules to achieve efficient ORR catalysts [39–43]. Passaponti *et al.* have investigated the physical properties of carbon-based materials pyrolyzed from tire granules [39] and the ORR activity of those carbons doped with Co and Cu [40]. Kang *et al.* [42] and Lee *et al.* [43] studied different pre-treatments on waste tire powders before pyrolysis and described their effect on the ORR of the obtained nitrogen-doped catalysts. Muhyuddin *et al.* [41] used microwave-assisted pyrolysis to synthesize a Fe-N-C catalyst from waste tires and investigated the ORR activity of synthesized catalysts in acidic, neutral and alkaline solutions.

1.4. The oxygen reduction reaction and the rotating disk electrode method

The oxygen reduction reaction (ORR) is the principal reaction that occurs on the cathode catalyst of a fuel cell. In its simplest form, the ORR can proceed via a so-called direct 4-electron process, whereby an oxygen molecule is directly chemisorbed onto the reaction center of a catalyst and is reduced by four electrons [8]:

$$O_2 + 2H_2O + 4e^- \rightarrow 4OH^- \quad (1)$$

Reaction (1) takes place in an alkaline medium and forms only hydroxide ions as a product. However, on Fe-N/C type catalysts, the ORR is proposed to be a more complex reaction that can happen via different pathways, each having many elementary reactions [3,26]. While the exact mechanism of this is debated, Ramaswamy and Mukerjee [26] propose that OH^- ions adsorbed onto the Fe-N/C reaction centers block the O_2 from reaching the reaction center, thereby promoting an outer-sphere electron transfer. In its simplified form, oxygen first undergoes a two-electron reduction leading to the formation of a peroxide anion as an intermediate [3]:

$$O_2 + H_2O + 2e^- \rightarrow HO_2^- + OH^- \quad (2)$$

In the second step, the peroxide anion can be reduced to OH^- [3]:

$$HO_2^- + H_2O + 2e^- \rightarrow 3OH^- \quad (3)$$

Reactions (1) and (2) together form a so-called 2+2-electron pathway, also called a four-electron series pathway, where $n = 4$. The ORR on Fe-N/C catalysts in alkaline media usually proceeds through the 2+2-electron pathway [3]. If reaction (2) is sluggish, some of the peroxide is not reduced and, as a result, peroxide may stay in the electrolyte solution. This is not favored, because the presence of peroxide decreases membrane and catalyst stability in fuel cells [7]. Additionally, the ORR activity suffers when reaction (2) does not fully occur. Therefore, catalyst properties need to be tuned for a full four-electron ORR to take place.

The rotating disk electrode (RDE) method is commonly used to estimate the ORR activity of the catalyst materials. The RDE measurements are performed in a three-electrode system consisting of a working electrode, a reference electrode, and a counter electrode placed into an electrolyte solution. The RDE, which acts as the working electrode, is a cylindrical electrode made from glassy carbon, graphite, gold, or platinum and surrounded by a sleeve made from an isolator such as Teflon. The tip of the RDE is covered with a thin layer of catalyst material, placed into the electrolyte solution, and rotated at a fixed rate using a rotator. The rotation introduces convection of the electrolyte solution and a diffusion-convection layer is formed near the electrode surface. The thickness of the diffusion-convection layer is proportional to the rotating rate of the electrode [44]. Using the RDE system, current density (j) vs electrode potential (E) curves (voltammograms) are measured at different rotation rates at a fixed electrode potential scan rate (mV s^{-1}). RDE voltammograms take a distinct shape where three regions are typically identified: the kinetic, mixed, and diffusion-limited regions.

In the kinetic region of the voltammogram the reaction rate is limited by charge transfer and the current density is independent of the electrode rotation rate. In the mixed kinetics region, the reaction rate is limited by both oxygen diffusion and charge transfer. In the diffusion-limited region, the reaction is solely limited by oxygen diffusion, causing the current density to depend on the electrode rotation rate (the thickness of the diffusion-convection layer) but not on the electrode potential. [44] In the diffusion-limited region, the Levich equation applies [44]:

$$j_d = 0.620\, n\, F\, D_O^{\frac{2}{3}}\, \omega^{\frac{1}{2}}\, \vartheta^{-\frac{1}{6}}\, C_O^0 \quad (4)$$

where j_d is the diffusion current density (A m^{-2}), n is the number of electrons transferred in the reaction, F is the Faraday's constant (C mol^{-1}), ω is the rotation rate of the electrode (rad s^{-1}), ϑ

is the kinematic viscosity of solution ($cm^2\ s^{-1}$), C_O^0 is the oxygen concentration in the solution ($mol\ m^{-3}$) and D_O is the oxygen diffusion coefficient in the solution ($cm^2\ s^{-1}$). In 0.1 M KOH solution at T = 25 °C, the values of these parameters are ϑ = 0.01 $cm^2\ s^{-1}$, C_O^0 = 1.2 $mol\ m^{-3}$ and D_O = 1.9 x 10^{-5} $cm^2\ s^{-1}$ [45]. These values were also used in this work. In the diffusion-limited region, the dependence between the diffusion current density j_d and the square root of the electrode rotation speed $\omega^{0.5}$ is linear. From this linear dependence of j_d and $\omega^{0.5}$, other parameters of the Levich equation can be calculated (e.g. n, D_O, ϑ or C_O^0).

In addition to n, two other parameters used to characterize the ORR activity of a catalyst are the onset potential (E_{onset}) and the half-wave potential ($E_{1/2}$). E_{onset} is the potential value at j = -1 A m^{-2} and $E_{1/2}$ is defined as the potential value where $j = 0.5j_d$. The more positive the onset and half-wave potentials, the more active the catalyst. [44]

While the RDE method is a simple and quick way to obtain a first idea of a catalyst's electrochemical activity, the rotating ring disk electrode (RRDE) and fuel cell tests are also used to evaluate the ORR activity and catalyst performance. Based on the RRDE data, in addition to the number of transferred electrons, the percentage yield of peroxide formation during the ORR process can be calculated. [46] A two-electrode system is often used to get a more realistic image of a catalyst's behavior. Since the two-electrode system's measurements take longer and require much more material to make the electrodes, they are usually performed only after good results are obtained using simpler methods such as the RDE or RRDE method.

1.5. Methods used for the physical characterization of materials

The physical characteristics of an ORR catalyst play an important role in achieving the best electrochemical activity possible. As mentioned in Chapter 1.2, the specific surface area and porosity are important characteristics for the formation of active centers and to enable ORR reactant access to active centers. Additionally, knowing the chemical composition of the catalyst is important for understanding the electrochemical behavior of catalysts (Chapter 1.3). Several methods exist to explore the physical characteristics of NPGM catalysts.

Low-temperature nitrogen sorption analysis provides information about the material's specific surface area and porosity. A sample is placed in a sealed container in a vacuum, which removes any adsorbed matter from the sample's surface. The container and sample are cooled to liquid nitrogen temperature (T = 77 K). Nitrogen gas is added to the container in controlled amounts and the nitrogen gas will adsorb onto the surface of the sample and into its pores. After an amount of N_2 is added, the pressure inside the container is measured. Plotting the obtained

partial pressure against the amount of adsorbed nitrogen gas results in an isotherm curve. It is possible to calculate parameters relating to pore and surface characteristics from this curve using, for example, the Brunauer-Emmet-Teller (BET) theory and the two-dimensional non-local density functional theory for heterogeneous surfaces (2D-NLDFT-HS). [47]

High-resolution scanning electron microscopy (HR-SEM) enables the visualization of the micro- and nanoscale morphology of the catalyst materials. A focused electron beam is scanned over the sample, which interacts with the matter in the sample. Most commonly, secondary electrons are detected and the intensity of this signal is related to the topography and composition of the scanned area. A raster image is formed from the scanned region. Using an energy dispersive X-ray (EDX) detector in tandem with HR-SEM, a semi-quantitative analysis of the elemental composition of the scanned region can be gathered based on the characteristic X-rays of the atoms in the sample. This is called the scanning electron microscopy energy dispersive X-ray (SEM-EDX) analysis. [48]

X-ray diffraction spectroscopy (XRD) provides a more detailed overview of a sample's crystallographic structure and chemical composition. In the XRD method, the sample is subjected to an X-ray beam at specific angles. The interference of elastically scattered X-rays from the sample at a given beam angle results in a diffraction pattern, from which the chemical composition and other properties of the material can be calculated. [49] XRD data can give insight into the specific composition of impurities in catalysts.

2. Experimental

2.1. Synthesis of carbon materials

Two carbon materials were used in the synthesis of the Fe-N/C catalysts. Both carbon materials were synthesized from waste tire granules (Imdex A/S, Denmark). Steel and textile components had previously been removed by the manufacturer. In the first synthesis (Figure 2) the tire granules were pyrolyzed in a tube furnace (Carbolite) at 1000 °C in Ar for three hours. Then, the carbon material was ball-milled (FRITSCH pulverisette 6) for 2x15 min at 400 rpm using five zirconia balls with a diameter of 20 mm. The yield of this process was 36.8%, which is a similar result to what is described in the literature [15,27,42,43]. This material will be referred to as "**C1**".

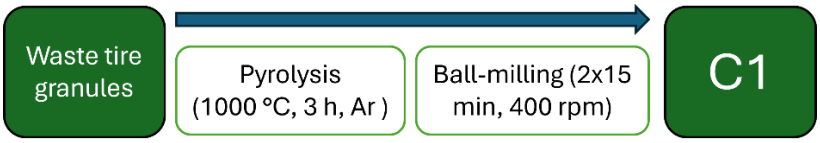

Figure 2. *Synthesis pathway of the carbon material C1.*

In the synthesis of the second carbon material (Figure 3), waste tire granules were first sonicated several times in MilliQ water. During the treatment, the water turned yellow, which indicated the removal of water-soluble compounds and dirt from the surface of the tire granules. The granules were dried and subsequently pyrolyzed at 450 °C for three hours in Ar. The SEM-EDX analysis of C1 showed that there were residues in the carbon, predominantly Si (Table 1 in Chapter 3.1.1), an alkaline treatment was carried out to remove the additives. The pyrolyzed carbon was treated in a 1 M KOH solution for one hour at 60 °C and flushed with MilliQ water to remove excess KOH and other compounds created during alkaline treatment. The material was then dried in a vacuum oven (T = 110 °C, P = 50 mbar). This material was synthesized by Annabel Raudsepp and will be referred to as "**C2**".

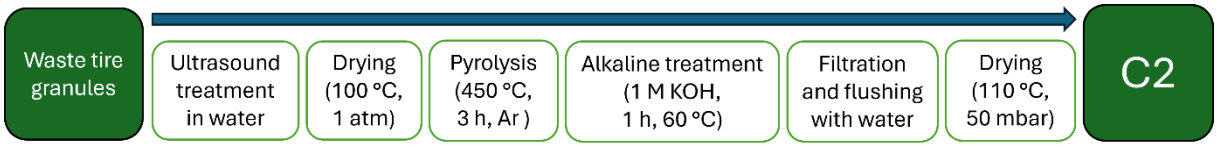

Figure 3. *Synthesis procedure of the carbon material C2.*

2.2. Synthesis of NPGM catalysts

A total of nine NPGM catalyst materials were synthesized. While precursors, precursor ratios, and some synthesis parameters were altered to obtain each material, the principal synthesis pathway remained the same, as summarized in Figure 4.

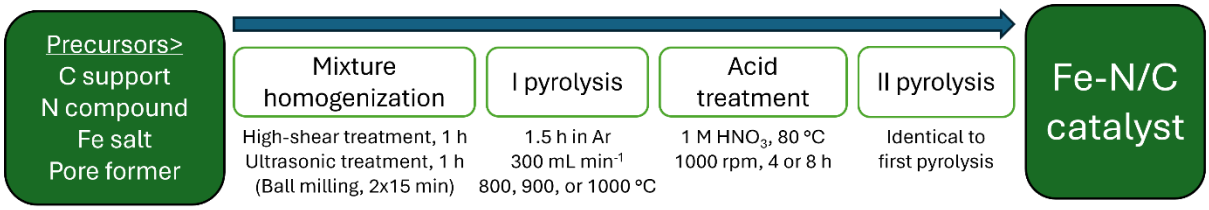

Figure 4. *Simplified overview of the NPGM catalyst synthesis pathway.*

In the catalyst synthesis, C1 or C2 was used as the carbon material. Guanidine carbonate (Sigma-Aldrich, 99%) or dicyandiamide (Sigma-Aldrich, 99%) was used as the nitrogen source and $Fe(NO_3)_3 \cdot 9H_2O$ (Sigma-Aldrich, ≥ 99.0%) was used as the iron salt. Additionally, $ZnCl_2$ (anhydrous, ACS reagent, ≥ 97%, Sigma-Aldrich) and acicular hydroxyapatite ($Ca_{10}(PO_4)_6(OH)_2$, ≥ 96%, 60 ± 10 nm particle size, Sigma-Aldrich) were used as pore formers.

First, the precursors were mixed with a minimal amount of ethanol. The mixture was homogenized using a high-shear mixer (IKA T25 ULTRA TURRAX) for one hour and sonicated in an ultrasound bath for another hour. For some materials, an additional ball-milling step (2x15 min, reversed, at 350 rpm) preceded the high-shear mixing. The homogenized mixtures were dried (P = 1 atm, T = 70 °C) and pyrolyzed for 1.5 hours at a temperature of 800, 900, or 1000 °C in Ar. Before pyrolysis, the tube furnace was flushed with Ar for 45–60 min at 200–300 ml min^{-1}. After pyrolysis, the materials were treated with 1 M HNO_3 solution (at 80 °C at a stirring rate of 1000 rpm) to remove unwanted residual elements present in waste tires as additives (Zn, S, Ca, and others) as well as residual unreacted Fe from the Fe salt and residual Zn from the $ZnCl_2$. After acid treatment, each material was washed with MilliQ water several times and filtered. The pH of the solution was checked with a pH indicator to confirm that all residual acid had been removed. Finally, each material was dried (P = 50 mbar, T = 60–80 °C) and pyrolyzed for a second time at identical conditions to the first pyrolysis.

To differentiate between all nine catalysts in this work, the materials were named according to their composition and main synthesis parameters. The first material, **Fe-DCDA/C1-I-800**, was synthesized using dicyandiamide (denoted as "DCDA" in the material's name) as the nitrogen precursor and C1 as the carbon source. In the material's name, "I" refers to precursor mass ratios (m(nitrogen compound) : m(iron salt) : m($ZnCl_2$) : m(carbon material) = 10:1:10:1) and the number "800" refers to the pyrolysis temperature (800 °C) used for both pyrolysis steps.

The material was subjected to acid treatment after the first pyrolysis for four hours. Finally, it was pyrolyzed for a second time at identical conditions to the first pyrolysis.

For the next material (**Fe-guan/C1-I-800**)**,** guanidine carbonate ("guan") was used instead of dicyandiamide as the nitrogen compound. Since SEM-EDX analysis of Fe-DCDA/C1-I-800 indicated that unwanted additives were not effectively removed (Chapter 3.1.2), a longer acid treatment duration of eight hours was chosen for this and all subsequent materials.

To compensate for a drop in nitrogen content (Chapter 3.1.2), **Fe-guan/C1-II-800** was synthesized using twice the amount of nitrogen compound (m(nitrogen compound) : m(iron salt) : m($ZnCl_2$) : m(carbon material) = 20:1:10:1).

The next two materials were synthesized at increased pyrolysis temperatures of 900 °C (**Fe-guan/C1-II-900**) and 1000 °C (**Fe-guan/C1-II-1000**). According to published data [30,34] increasing the pyrolysis temperature from 800 °C to 900–1000 °C yields higher ORR activity for NPGM catalysts.

Two more materials were synthesized using hydroxyapatite ("HA") as an additional pore former (mass ratio 10:1 compared to C1) at 900 °C (**Fe-guan/C1-II-900-HA**) and 1000 °C (**Fe-guan/C1-II-1000-HA**). Teppor *et al.* [11,30] have shown that the use of a hard-templating agent (HA) in the synthesis of NPGM catalysts increases meso- and macroporosity, enhancing O_2 mass transport in the material and improving ORR activity.

Lastly, two materials were synthesized using C2 as the carbon material instead of C1, at 900 °C (**Fe-guan/C2-II-900**) and 1000 °C (**Fe-guan/C2-II-1000**).

2.3. Physical characterization methods

HR-SEM (Zeiss Merlin, 4 kV) was used to study the morphology and structure of the materials. SEM-EDX (Bruker EDX-Xflash®, 8 kV) was used in tandem with HR-SEM to study the materials' elemental composition. Before measurement, samples were prepared by pipetting the material in an isopropyl alcohol suspension onto carbon tape and left to dry at room temperature. The samples were covered with a thin layer of Au/Pd (layer thickness d = 0.5 nm). HR-SEM and SEM-EDX measurements were conducted under the supervision of PhD Olga Volobujeva at the Institute of Materials and Environmental Technology at Tallinn University of Technology.

The porosity of the carbon materials and NPGM catalysts was analyzed using the nitrogen sorption method (Micromeritics 3Flex). The samples were degassed overnight at 0.05 mbar at 100 °C. Measurements were carried out at liquid nitrogen temperature (T = 77 K). Specific

surface area (S_{BET}) values of the materials were calculated according to the Brunauer-Emmett-Teller theory (BET). The total pore volumes (V_{tot}) of the samples were determined from the isotherm at the relative pressure of nitrogen of 0.95. The two-dimensional non-local density functional theory for heterogeneous surfaces (2D-NLDFT-HS) was used to calculate specific surface area values (S_{DFT}), the volume of micropores (V_{micro}), and total pore volume values (V_{DFT}) using SAIEUS software. This software was also used to calculate pore size distributions.

XRD was used to further study the composition of some materials using a Bruker D8 Advanced diffractometer, which was equipped with a Ni-filtered Cu Kα X-ray source. Topaz software was used to obtain diffraction patterns. The XRD measurements were conducted by MSc Jaan Aruväli at the University of Tartu Institute of Ecology and Earth Sciences.

2.4. Electrochemical characterization of carbon materials and NPGM catalysts

The rotating disk electrode method (RDE) was used to characterize the kinetics of the ORR on each material in a three-electrode cell. A glassy carbon disk electrode (GCDE) coated with a suspension of synthesized catalyst was used as the working electrode. The GCDE was cleaned using alumina powder (BUEHLER Micro Polish), washed with Milli-Q water, and dried. A suspension of the catalyst material, isopropyl alcohol (99,99%, Lachner, s.r.o.), MilliQ water, and Nafion® 117 (~5% suspension, Sigma-Aldrich, Aldrich Chemistry) solution was treated with a high-shear mixer for one hour and an ultrasound bath for another hour. The suspension was then pipetted onto the GCDE and left to dry at room temperature. The loading of each electrode was approximately 0.30 mg cm^{-2}.

The RDE measurements were conducted in a 0.1 M KOH solution (99.99% KOH pellets, semiconductor grade, Sigma-Aldrich). A reversible hydrogen electrode (RHE) was used as the reference electrode and a carbon rod was used as the counter electrode. Before measurements, all glassware was washed with a mixture of concentrated H_2SO_4 (95-98%, ACS Reagent, Sigma-Aldrich) and a small amount of H_2O_2 solution (30%), heated to 90 °C. All potentials in this work are presented relative to the RHE.

A rotator (Pine Instrumental Company) and a Gamry Reference 600TM potentiostat (Gamry Instruments) were used to perform the measurements. First, the electrode was cycled in the potential range of E = 0.23–1.25 V vs RHE in Ar (99.9999%, AS Linde Gas) saturated solution for at least seven cycles. Then, at least seven more voltammograms are measured in the same potential range in O_2 (99.999%, AS Linde Gas) saturated solution. The RDE method was used to measure current density versus electrode potential curves at electrode rotation rates

of 500–3000 rpm in the potential range of E = 0.23–1.25 V vs RHE and at a potential scanning rate of v = 10 mV s^{-1}. j vs E curves were measured in an O_2-saturated solution and after saturating the solution with Ar, the j vs E curves were measured in Ar saturated solution.

Electrochemical impedance spectroscopy (EIS) was performed to determine the solution's resistance. This value (43 ± 4 Ω) was used to compensate for the ohmic potential drop. Additionally, all current density values measured in an O_2-saturated solution are corrected to those measured in an Ar-saturated solution.

3. Results and discussion

3.1. Physical characterization

Three methods were used for the physical characterization of all materials: N_2 sorption analyses gave insight into the materials' porosity, HR-SEM provided information on surface characteristics, and SEM-EDX was used to determine elemental composition. XRD was used to further investigate the composition of some of the catalyst materials.

3.1.1. Physical characterization of carbon materials

HR-SEM images (Figure 5) show that both carbon materials are porous. C1 and C2 appeared to be composed of particles of varying sizes, with smaller ones surrounding larger particles. In general, the materials look quite similar and consist of small, round carbon particles.

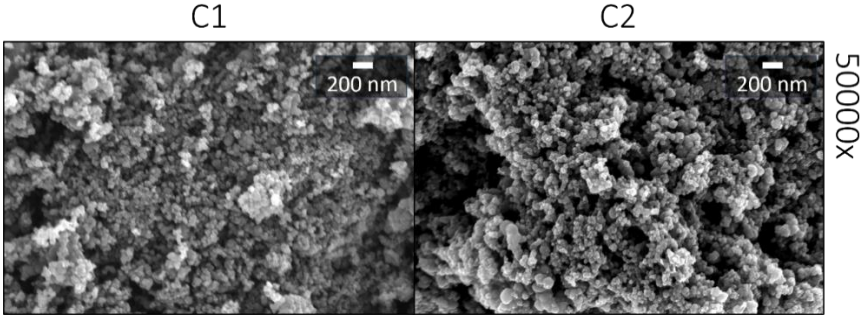

Figure 5. *HR-SEM images of carbon materials C1 and C2, 50000x magnification.*

According to SEM-EDX analyses (Table 1), both carbon materials contained various impurities in addition to carbon and oxygen, such as Si, S, Ca, and Zn. SiO_2 and $CaCO_3$ are common filler materials in tires and Zn and S are left from the vulcanization process of tire rubber [15,27,35,36,50]. Impurities such as Mg and Ca ions may have an unfavorable effect on the ORR activity because they are good hydrogen peroxide stabilizers [51]. Additional thermogravimetric analyses [52] showed that C1 had an ash content of 18.4 wt% which is in accordance with what is described in the literature. [15,27,35] C1 has a considerable amount of Si, while the alkaline treatment used in the synthesis of C2 effectively removed most of the Si. However, the presence of K in C2 material may be residuals from the same KOH treatment.

C2 has a noticeable amount of Zn, possibly because the pyrolysis temperature of C2 is much lower compared to C1. Conesa *et al.* analyzed chars from pyrolyzing waste tires at 450 °C and 1000 °C and found that Zn content was much lower in the char when pyrolyzing waste tires at 1000 °C (6.7 wt% Zn) compared to 450 °C (0.9 wt% Zn). They argued that in the presence

of hydrogen or methane gas (which both are produced during pyrolysis of waste tires), ZnO could transform into metallic Zn and evaporate (the boiling point of Zn is 901 °C). [53]

Table 1. *SEM-EDX analysis results for carbons C1 and C2 (in wt%).*

Material	C	O	Si	Zn	S	Ca	K	Other (<0.5%)
C1	79	10.5	6.9	0.71	1.6	0.72	-	Mg, Al
C2	81	9.5	1.1	4.2	2.0	0.55	1.1	Mg, Al

N_2 sorption analysis for the carbons (Table 2) shows that C1 had twice the specific surface area (S_{BET} = 125 m^2 g^{-1}) compared to C2 (S_{BET} = 59 m^2 g^{-1}), larger total pore volume, and a higher microporosity ratio (V_{micro}/V_{DFT} = 13% vs 8%). This shows that C1 is significantly more microporous than C2. Carbon black obtained from pyrolyzing waste tires at lower temperatures is known to have residues of rubber and tire pyrolysis oil adsorbed onto the carbon black surface, which could clog pores and reduce the surface area whereas using higher pyrolysis temperatures removes those residues and results in a more porous material [15,27,35,53]. Martinez *et al*. [15] reviewed papers on the pyrolysis of waste tires at different conditions and found that waste tire carbons pyrolyzed at 500-600 °C had a S_{BET} of 61-89 m^2 g^{-1}, which is in a similar range as C2.

Table 2. *N_2 sorption results of carbons C1 and C2: Specific surface area (S_{BET}) according to BET calculations and total volume of pores (V_{tot}), and parameters calculated with SAIEUS software according to 2D-NLDFT-HS: specific surface area (S_{DFT}), micropore volume (V_{micro}), total volume of pores (V_{DFT}).*

Material	S_{BET} m^2 g^{-1}	S_{DFT} m^2 g^{-1}	V_{tot} cm^3 g^{-1}	V_{DFT} cm^3 g^{-1}	V_{micro} cm^3 g^{-1}	V_{micro} /V_{DFT}
C1	125	116	0.27	0.23	0.030	0.13
C2	59	40	0.16	0.14	0.011	0.08

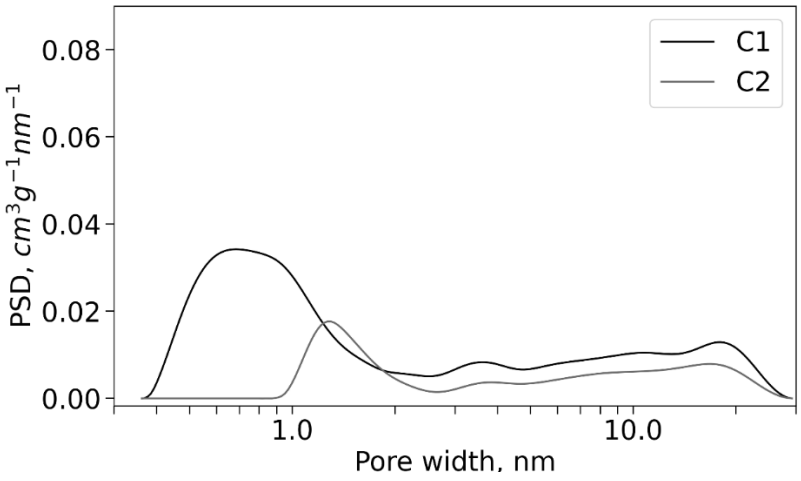

Figure 6. *Pore size distribution of carbons C1 and C2.*

Figure 6 presents pore size distributions of the carbon materials and confirms that not only does C1 have a higher overall porosity, but it is indeed much more microporous. Moreover, C1 has so-called ultramicropores, with most pores having a diameter d < 1 nm, while the micropores in C2 have a diameter d = 1–2 nm.

Carbons synthesized from waste tires tend to have a lower surface area and porosity [15,27,39,41] compared to other carbon sources, such as peat [11,12].

3.1.2. Physical characterization of NPGM catalyst materials

First, it was examined how different N precursors and their amount affect the surface structure of NPGM catalysts. HR-SEM images (Figure 7) show that Fe-DCDA/C1-I-800, Fe-guan/C1-I-800 and Fe-guan/C1-II-800 have a porous, granular morphology. Particles of diverse sizes are present where larger particles are enveloped by smaller ones, potentially enhancing the oxygen mass transport rate [54]. It is observed that Fe-guan/C1-II-800 exhibits larger, distinct agglomerates with more pronounced free space surrounding them.

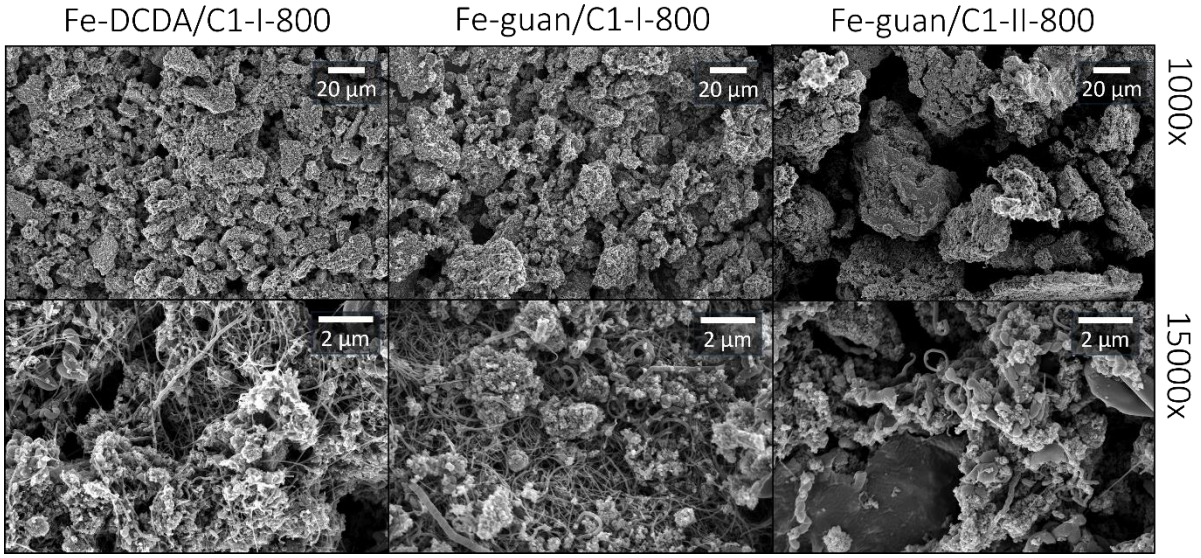

Figure 7. *HR-SEM images for NPGM catalysts with different N precursors and precursor ratios at 1000x and 15000x magnification.*

At higher magnification, all these materials show an extensive network of nanofibers. Those fibers were confirmed to have a nearly identical elemental composition compared to the bulk material (C ~ 80 wt%, Fe ~ 4 wt%, and N ~ 8 wt% for Fe-DCDA-I-800 according to SEM-EDX). The HR-SEM images suggest that no change in nanofiber formation is observed when synthesizing NPGM materials using a different N precursor, however, Fe-guan/C1-II-800, which was synthesized with a higher mass ratio of N to C precursors (20:1 compared to 10:1), has a lower number of nanofibers compared to Fe-guan/C1-I-800. The formation of

nanofibers is well-known in N-doped carbons [55] and is dependent on the precursors and precursor ratios used [54,56]. The presence of such nanofibers is believed to improve the stability and mass-transfer properties of the catalyst [54,55].

HR-SEM analyses also suggest that changing the pyrolysis temperature (800, 900, and 1000 °C) does not noticeably influence the surface structure of the catalysts (Figure 8).

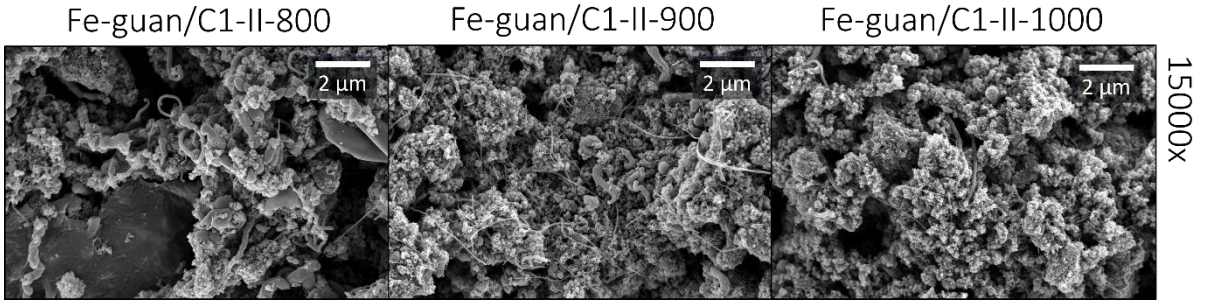

Figure 8. *HR-SEM images of NPGM catalysts at different pyrolysis temperatures (all other synthesis parameters are identical) at 15000x magnification.*

Nanofibers are present in the materials even when changing the pyrolysis temperature, nitrogen compound, and precursor ratios. Using hydroxyapatite (HA) as an additional pore former in the synthesis process (Fe-guan/C1-II-900 and Fe-guan/C1-II-1000), the formation of nanofibers in the material is no longer observed (Figure 9).

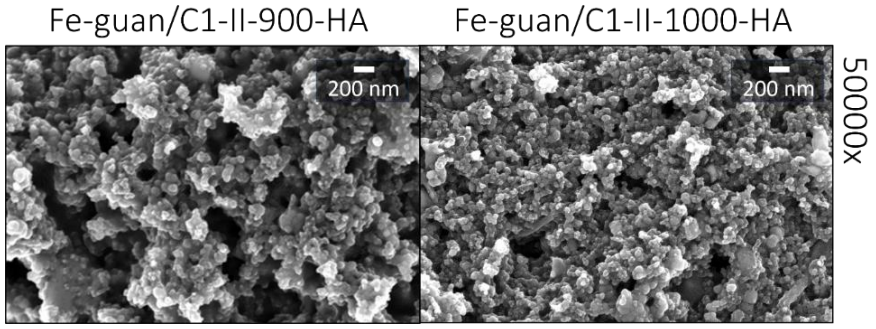

Figure 9. *HR-SEM images of catalyst materials synthesized using hydroxyapatite as an additional pore former at 50000x magnification.*

The two catalysts synthesized using C2 as the carbon support (Fe-guan/C2-II-900 and Fe-guan/C2-II-1000) show a similar surface structure compared to that of Fe-guan/C1-II-900. Nanofibers are also present in similar amounts (Figure 10).

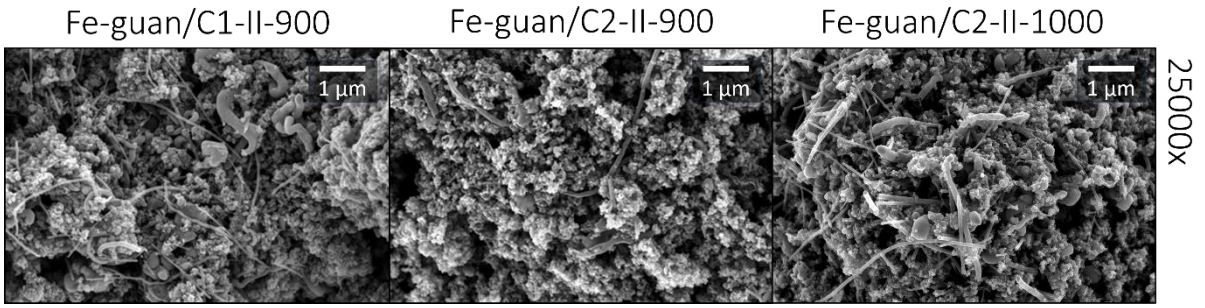

Figure 10. *HR-SEM images for catalysts synthesized using C2 as carbon support compared to Fe-guan/C1-II-900 at 25000x magnification.*

SEM-EDX results for all synthesized NPGM catalysts are shown in Table 3. Up to three different spots were measured on each material and the results were averaged and rounded.

Table 3. *SEM-EDX analysis results of all NPGM catalysts (wt%).*

Material	**C**	**O**	**Fe**	**N**	**P**	**Other (1-5%)**	**Other (< 1%)**
Fe-DCDA/C1-I-800	78	8.0	4.2	7.1	-	Si, Zn	Cl
Fe-guan/C1-I-800	75	12	3.9	4.2	-	Si	Al, S, Zn
Fe-guan/C1-II-800	75	10	3.2	6.7	-	Si, Zn	-
Fe-guan/C1-II-900	75	9.0	4.2	6.0	-	Si	Al, S, Zn
Fe-guan/C1-II-1000	76	8.8	3.5	4.7	-	Si, S	Al, Zn
Fe-guan/C1-II-900-HA	69	18	5.4	-	6.1	-	Al, Ca, Mg, Si, Zn
Fe-guan/C1-II-1000-HA	84	8.3	3.4	-	1.6	Ca	Cl, Si
Fe-guan/C2-II-900	85	7.0	4.4	2.2	-	-	S, Si
Fe-guan/C2-II-1000	82	13	2.4	2.0	-	-	S, Si

Fe-DCDA/C1-I-800 has, in addition to carbon and oxygen, a noticeable amount of Fe and N, proving the doping of the carbon effective. Some Zn and Si is also present, which comes from the carbon material. Some Zn along with Cl may have been left in the material from the $ZnCl_2$ precursor and was not removed by the acid treatment. The acid treatment time was therefore increased from 4 h to 8 h for the next material to remove more impurities.

Fe-guan/C1-I-800 shows a significantly lower Zn content compared to Fe-DCDA/C1-I-800 and therefore the acid treatment time was fixed at 8 h for all subsequent syntheses. Another difference between the two catalysts is a lower N content in Fe-guan/C1-I-800. To increase the N content and thereby boost activity toward the ORR, the amount of nitrogen precursor was doubled in the synthesis of Fe-guan/C1-II-800. SEM-EDX results show that more N was indeed detected in Fe-guan/C1-II-800 compared to Fe-guan/C1-I-800.

The pyrolysis temperature was the only parameter changed in the synthesis of Fe-guan/C1-II-900 and Fe-guan/C1-II-1000 compared to Fe-guan/C1-II-800. N content is lower when using

higher pyrolysis temperatures, which has also been observed in other studies [57,58]. Higher pyrolysis temperatures also remove more residual Zn.

To further improve mesoporosity, two materials were synthesized using additional pore former hydroxyapatite – Fe-guan/C1-II-900-HA and Fe-guan/C1-II-1000-HA. All other precursor ratios remained unchanged compared to Fe-guan/C1-II-900 and Fe-guan/C1-II-1000, respectively. Surprisingly, nitrogen was not detected in these catalysts. Instead, a noticeable amount of phosphorus was present. Hydroxyapatite ($Ca_{10}(PO_4)_6(OH)_2$) contains P in its structure, which may have been incorporated in the carbon structure and was not removed with acid treatment. Additional XRD analyses (Figure 11) confirmed that both catalysts contained phosphorus compounds: Fe-guan/C1-II-900-HA contained mostly $Fe(PO_3)_2$, and Fe-guan/C1-II-1000-HA contained FeP.

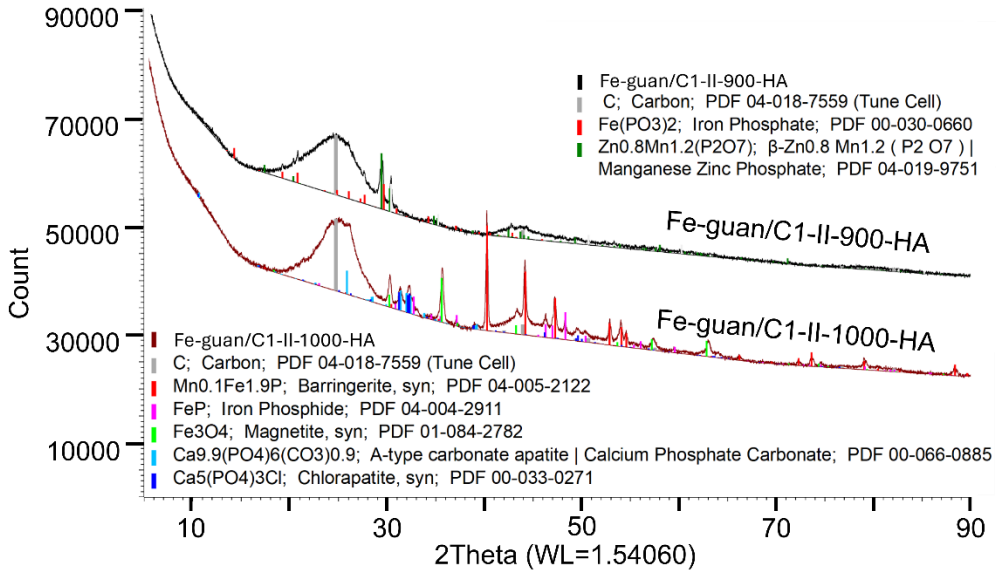

Figure 11. *XRD results for Fe-guan/C1-II-900-HA and Fe-guan/C1-II-1000-HA.*

For the last two materials, C2 was used in the catalyst synthesis as the carbon support. C2 contained fewer impurities than C1 because of the additional alkaline treatment step. As a result, the C2-based catalysts also contain fewer impurities, as is evident in

Table ***3***, when comparing Fe-guan/C2-II-900 with Fe-guan/C1-II-900 and Fe-guan/C2-II-1000 with Fe-guan/C1-II-1000. Additionally, they contain significantly less nitrogen than materials synthesized using C1.

The porous structure of the synthesized catalysts was studied more extensively with the nitrogen sorption method. The results, presented in Table 4, show that the catalysts have specific surface area values below 193 $m^2\ g^{-1}$. While the specific surface area of NPGM catalysts synthesized from waste tire carbons is generally rather low and the specific synthesis

pathway can significantly affect a catalyst's surface area. For example, Kang *et al.* [42] and Lee *et al.* [43] presented NPGM catalysts based on waste tire carbons exhibiting S_{BET} values ranging from 65 to 494 $m^2\ g^{-1}$. Muhyuddin *et al.* [41] presented waste tire carbon based Fe-N/C catalysts with S_{BET} from 85 to 204 $m^2\ g^{-1}$, whereby the catalyst with the lowest specific surface area and porosity yielded the highest ORR activity in an alkaline solution.

Table 4. *N_2 sorption results of NPGM catalysts: specific surface area according to BET calculations (S_{BET}), and the total volume of pores (V_{tot}) according to 3FLEX calculations; and parameters calculated with SAIEUS software according to 2D-NLDFT-HS: specific surface area (S_{DFT}), micropore volume (V_{micro}), and the total volume of pores (V_{DFT}).*

Material	S_{BET} $m^2\ g^{-1}$	S_{DFT} $m^2\ g^{-1}$	V_{tot} $cm^3\ g^{-1}$	V_{DFT} $cm^3\ g^{-1}$	V_{micro} $cm^3\ g^{-1}$	V_{micro}/V_{DFT}
Fe-DCDA/C1-I-800	99	88	0.18	0.17	0.023	0.14
Fe-guan/C1-I-800	153	146	0.21	0.19	0.054	0.28
Fe-guan/C1-II-800	174	156	0.24	0.22	0.047	0.21
Fe-guan/C1-II-900	77	72	0.11	0.11	0.024	0.22
Fe-guan/C1-II-1000	156	143	0.25	0.24	0.043	0.18
Fe-guan/C1-II-900-HA	39	37	0.08	0.07	0.011	0.16
Fe-guan/C1-II-1000-HA	75	63	0.16	0.14	0.018	0.13
Fe-guan/C2-II-900	153	146	0.23	0.20	0.045	0.23
Fe-guan/C2-II-1000	193	169	0.25	0.24	0.053	0.22

A few trends can be noted when comparing the pore characteristics of the catalysts. Firstly, Fe-DCDA/C1-I-800 has a lower specific surface area than Fe-guan/C1-I-800. Fe-DCDA/C1-I-800 shows a very slight shift toward microporosity while Fe-guan/C1-I-800 is more microporous (Figure 12a). The only synthesis parameter that was changed was the nitrogen compound, which means that the choice of N precursor has a significant effect on porosity.

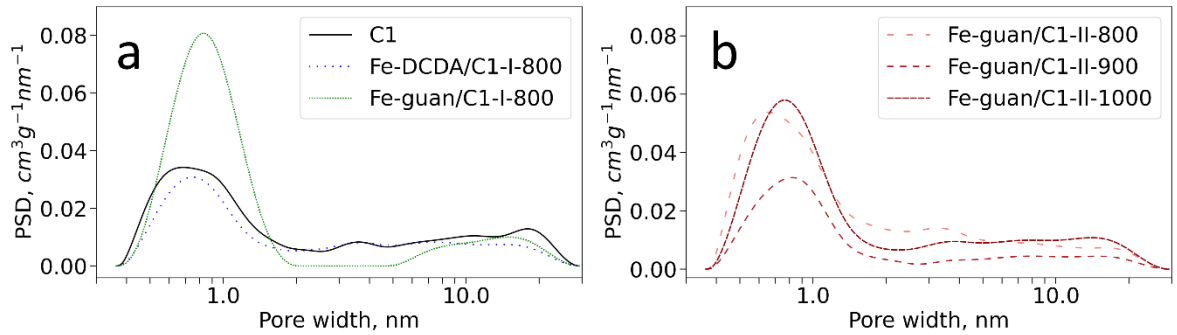

Figure 12. *Pore size distribution of the NPGM catalysts: (a) materials with different N precursors along with C1 and (b) Fe-guan/C1-II materials synthesized at different pyrolysis temperatures.*

The second visible trend is the effect of the pyrolysis temperature on the porosity. The materials pyrolyzed at 1000 °C have a higher specific surface area than their respective

counterparts synthesized at 900 °C. This temperature dependence is also observed in the pore size distribution plots (Figure 12b and Figure 13). An increase in surface area at higher pyrolysis temperatures is also described in the literature [27,53].

Although HR-SEM images (Figure 9) suggested that Fe-guan/C1-II-900-HA and Fe-guan/C1-II-1000-HA are homogeneously porous materials, both materials have a much lower specific surface area compared to those synthesized without HA. The higher surface area in the other materials may be linked to the presence of nanofibers in all materials that were synthesized without HA. Still, pore size distributions (Figure 13a) show that the pores of Fe-guan/C1-II-900-HA are, on average, shifted toward the mesoporous region compared to other materials synthesized at 900 °C. Teppor *et al.* [30] found that for Fe-N/C materials synthesized using peat as a carbon source, the addition of HA as a pore former also somewhat shifted the average pore volume toward the mesoporous region.

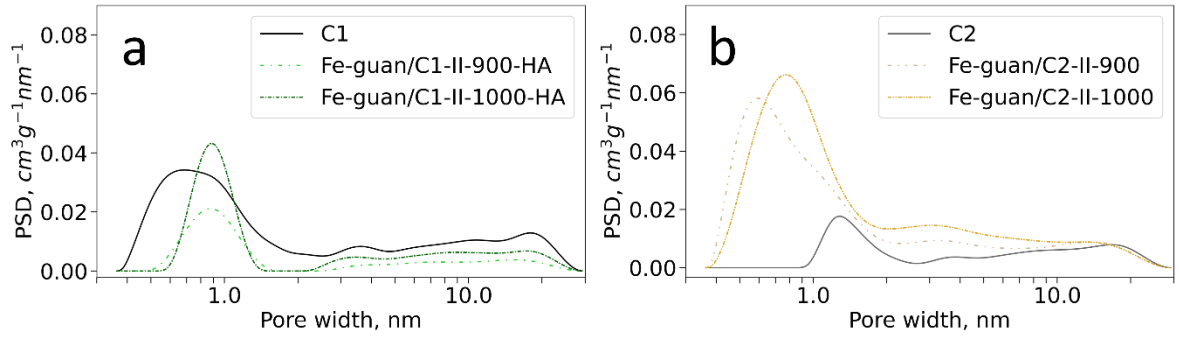

Figure 13. *Pore volume distribution of the catalysts (a) that were synthesized using HA as an additional pore former, along with C1, and (b) that were synthesized using C2 as carbon support, along with C2.*

Lastly, the specific surface areas and pore characteristics of Fe-guan/C2-II-900 and Fe-guan/C2-II-1000 did not significantly differ compared to the results of all other materials (Table 4 and Figure 13).

3.2. Electrochemical characterization

The RDE method was used to estimate the electrochemical activity of the ORR on the two carbon materials and the NPGM catalysts. Current density (*j)* versus electrode potential (*E*) curves were recorded in 0.1 M KOH solution at various electrode rotation rates.

Figure 14 shows cyclic voltammograms of carbons C1 and C2 measured in a solution saturated with Ar. The difference between cathodic and anodic sweep directions is much larger for C1 material than that for C2, which indicates a higher gravimetric capacitance. The gravimetric capacitance of porous carbon materials is linked to the area of the electric double

layer formed on the surface of the material. The larger the specific surface area of the material, the larger the electric double layer and also the gravimetric capacitance [59]. This result is coherent with the N_2 sorption results (Table 2), which show that C1 has a much larger S_{BET} value than C2.

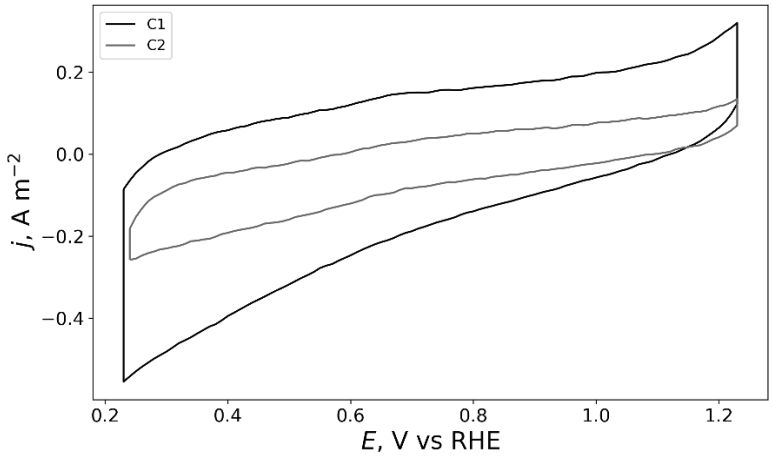

Figure 14. *Cyclic voltammogram of C1 and C2 at an electrode rotation rate of 2000 rpm in Ar saturated 0.1 M KOH solution.*

Figure 15 presents *j* vs *E* curves for the two carbon materials as well as Fe-N/C catalysts (noted in the figure) at an electrode rotation rate of 2000 rpm.

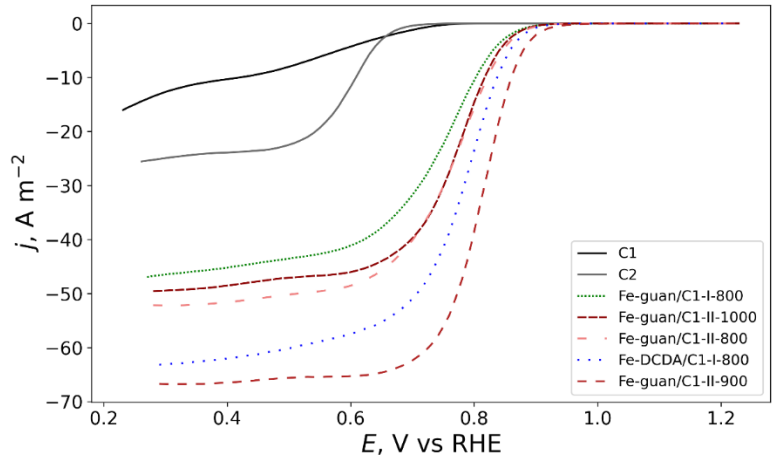

Figure 15. *Cathode-direction ORR curves of materials (noted in the figure) recorded at an electrode rotation rate of 2000 rpm in O_2 saturated 0.1 M KOH solution.*

From these curves, the onset potential (E_{onset}) was calculated for each material (Table 5). The onset potential is one way to quantitatively describe a material's activity toward the ORR. Another way to characterize a catalyst's activity toward the ORR is the number of transferred electrons (*n*) in the reaction, also presented in Table 5, which was calculated for each material using the Levich equation (equation (4)).

Table 5. *Onset potential values (E_{onset}), half-wave potentials ($E_{1/2}$), and the number of transferred electrons (n) in the ORR for all materials.*

Material	E_{onset} (V vs RHE)	$E_{1/2}$ (V vs RHE)	*n* value (Levich) (E = 0.3 V vs RHE)
C1	0.71 ±0.01	-	-
C2	0.68 ±0.01	0.60 ±0.01	1.4 ±0.2
Fe-DCDA/C1-I-800	0.90 ±0.01	0.78 ±0.01	3.7 ±0.2
Fe-guan/C1-I-800	0.88 ±0.01	0.75 ±0.01	2.7 ±0.2
Fe-guan/C1-II-800	0.89 ±0.01	0.76 ±0.01	3.1 ±0.2
Fe-guan/C1-II-900	0.92 ±0.01	0.81 ±0.01	4.0 ±0.2
Fe-guan/C1-II-1000	0.88 ±0.01	0.77 ±0.01	2.9 ±0.2
Fe-guan/C1-II-900-HA	0.86 ±0.01	0.70 ±0.01	3.0 ±0.2
Fe-guan/C1-II-1000-HA	0.84 ±0.01	0.69 ±0.01	3.5 ±0.2
Fe-guan/C2-II-900	0.86 ±0.01	0.73 ±0.01	3.4 ±0.2
Fe-guan/C2-II-1000	0.90 ±0.01	0.78 ±0.01	3.7 ±0.2

Firstly, it is evident from Figure 15 and Table 5 that C1 and C2 have rather low onset potentials and therefore a low activity toward the ORR. This is why modifying the carbons with Fe and N is necessary to increase the ORR activity. Using Fe and dicyandiamide (Fe-DCDA/C1-I-800) yielded a catalyst with a much higher activity toward the ORR, as characterized by a much higher E_{onset} value (0.9 V vs RHE), $E_{1/2}$, *n*, and a well-defined diffusion plateau. In the synthesis of the catalyst, replacing the N precursor DCDA with guanidine carbonate (Fe-guan/C1-I-800) led to an increase in the specific surface area (Table 4) but resulted in a less active material toward the ORR compared to Fe-DCDA/C1-I-800. This could be due to the lower N content in the catalyst (SEM-EDX analyses result in

Table 3). Fe-guan/C1-II-800 was synthesized using double the quantity of N precursor compared to Fe-guan/C1-I-800 leading to an increased nitrogen content in the catalyst (

Table ***3***) and a slight improvement in E_{onset} and $E_{1/2}$ values.

Next, elevating the pyrolysis temperature from 800 °C to 900 °C resulted in an excellent enhancement in ORR activity: the E_{onset} and $E_{1/2}$ values of Fe-guan/C1-II-900 were 30 mV and 50 mV higher, respectively, compared to Fe-guan/C1-II-800 and *n* values reached a value of four, which means that oxygen was reduced by a four-electron process. Further increasing the pyrolysis temperature to 1000 °C (Fe-guan/C1-II-1000) resulted in diminished ORR activity.

The ORR activity of the NPGM catalysts that were synthesized using hydroxyapatite as an additional pore former (Fe-guan/C1-II-900-HA and Fe-guan/C1-II-1000-HA) did not increase compared to their respective counterparts that were synthesized without HA (Fe-guan/C1-II-900 and Fe-guan/C1-II-1000) (Figure 16). The E_{onset} value of Fe-guan/C1-II-900-HA was 60

mV lower compared to Fe-guan/C1-II-900 and 40 mV lower for Fe-guan/C1-II-1000-HA compared to Fe-guan/C1-II-1000 (Table 5). The electrochemical activity of these catalysts might have suffered due to the lack of N and the presence of various P compounds, such as FeP and $Fe(PO_3)_2$, as discussed in Chapter 3.1.2 (SEM-EDX and XRD results). However, researchers have reported that P-containing catalysts show promising results for ORR [60–62]. For example, Norouzi *et al.* [60] synthesized a Fe-P catalyst using triphenylphosphine, iron(II) chloride, and $ZnCl_2$, which has competitive E_{onset} and $E_{1/2}$ values in 0.1 M KOH solution in comparison to commercial Pt/C catalyst.

There are possibilities to improve the synthesis method using HA as a pore former. For example, one way to increase the mesoporosity and generate active Fe-N_x centers could be to modify the carbon material with HA first, remove the additives (like P) from the carbon with acid treatment, and then synthesize the NPGM catalyst by modifying the carbon support with Fe and N compounds. Another possibility is to research synthesis pathways that leave both Fe-P and Fe-N_x active centers in the structures.

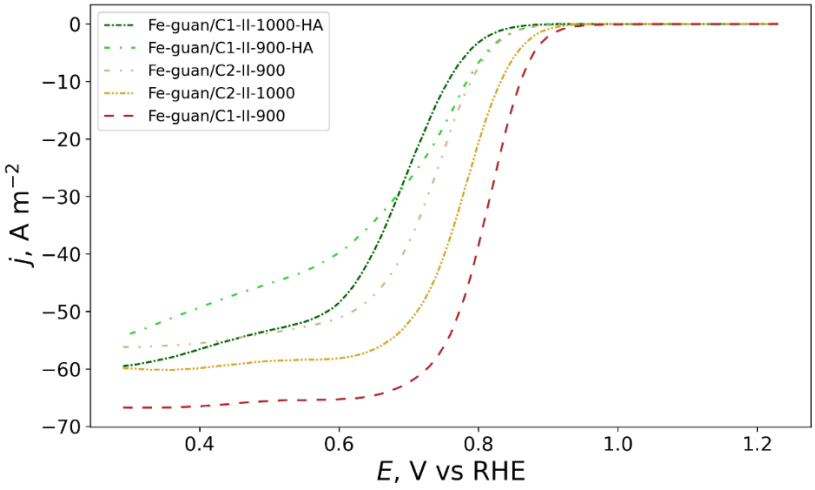

Figure 16. *Cathode-direction ORR curves of materials synthesized using additional pore former hydroxyapatite: Fe-guan/C1-II-900-HA and Fe-guan/C1-II-1000-HA; materials using C2 as carbon support: Fe-guan/C2-II-900 and Fe-guan/C2-II-1000; and Fe-guan/C1-II-900 at an electrode rotation rate of 2000 rpm in O_2 saturated 0.1 M KOH solution.*

C1 contained impurities that could negatively affect the materials' activity toward the ORR (SEM-EDX results in Table 1). C2, however, contained fewer impurities and could potentially be used to synthesize NGPM catalyst materials with a higher ORR activity. *j* vs *E* curves of Fe-guan/C2-II-900 and Fe-guan/C2-II-1000 (Figure 16) show that E_{onset} values are 60 mV and 20 mV lower, respectively, compared to Fe-guan/C1-II-900. From this, it can be concluded that when comparing materials synthesized using C1 as carbon support with the materials using C2, impurities in the carbon have minimal impact on the activity of the synthesized NPGM

materials. Instead, the specific surface area is the more critical factor. Therefore, it may also be the case that C1-based NPGM catalysts synthesized at a pyrolysis temperature of 900 °C yielded the best electrochemical results, using a pyrolysis temperature of 1000 °C yields better results for C2-based catalysts. The variance in behavior may be because C2 was pyrolyzed at 450 °C and has a specific surface lower than C1 which was synthesized at 1000 °C and has a higher S_{BET} value.

To summarize, when assessing all important electrochemical parameters (E_{onset}, $E_{1/2}$, and n), the top three NPGM catalyst materials are as follows: Fe-guan/C1-II-900 > Fe-DCDA/C1-I-800 ≈ Fe-guan/C2-II-1000. Fe-guan/C1-II-900 achieved an E_{onset} = 0.92 V vs RHE, $E_{1/2}$ = 0.81 V vs RHE, and n = 4. All other catalyst materials have somewhat lower E_{onset} and $E_{1/2}$ values and, additionally, the values of n of all catalyst materials were between two and four, indicating a 2+2-electron ORR.

The best result in this work achieved a similar or slightly more positive E_{onset} value (0.92 V vs RHE) compared to what is reported in the literature for similar materials. For example, Muhyuddin *et al.* [41] presented Fe-N/C catalyst synthesized from waste tire granules that achieved E_{onset} = 0.917 V vs RHE, whereas Lee *et al.* [43] and Kang *et al.* [42] achieved NPGM catalysts with E_{onset} = 0.9 V vs RHE. Interestingly, the best-performing ORR catalyst, Fe-guan/C1-II-900, has a lower S_{BET} value compared to other synthesized materials. The same tendency was presented by Muhyuddin *et al.* [41].

The onset potentials of commercial Fe-N/C catalyst material (PMF-12704, Pajarito Powder) or Pt-containing catalyst (20% Platinum on Vulcan XC-72, FuelCellStore) are 20 mV and 70 mV higher [30], respectively, compared to Fe-guan/C1-II-900, which was the best-performing catalyst for the ORR described in this work. The synthesis pathway of Fe-guan/C1-II-900 can therefore be further optimized to yield even better ORR activity.

In summary, it was shown that depending on the choice of precursors (carbon material and N compound), precursor ratios, and synthesis parameters (e.g. pyrolysis temperature), the resulting catalyst materials exhibited very different electrochemical behavior. Fe-guan/C1-II-900 is very suitable for further studies in single-cell tests.

4. Conclusions

This work aimed to develop Fe-N/C catalyst materials for efficient oxygen reduction in an alkaline solution. Nine catalysts were synthesized by mixing carbon derived from waste tire granules, iron salt, a nitrogen compound, and pore former ($ZnCl_2$). The mixture was homogenized, pyrolyzed, treated with an acid solution, and pyrolyzed for a second time. Several synthesis parameters were altered to obtain different catalysts:

1) Two carbon materials, C1 and C2, were used – waste tire granules were pyrolyzed at 1000 °C (C1), and at 450 °C with additional alkaline treatment for C2;
2) Two nitrogen precursors were used – guanidine carbonate or dicyandiamide;
3) Different mass ratios of nitrogen compound to carbon were selected: 10:1 and 20:1;
4) The temperature of the pyrolysis was varied – 800, 900, or 1000 °C;
5) A second pore former – hydroxyapatite (HA) – was added to the synthesis mixture.

The materials' ORR activity was investigated in 0.1 M KOH solution using the RDE method.

Physical characterization of the carbons (HR-SEM and SEM-EDX) revealed that C1 contained numerous impurities originating from the waste tire granules (Si, S, Ca, Zn, Mg, Al), whereas C2 contained considerably fewer impurities due to the additional alkaline treatment step. Both carbon materials were microporous and the specific surface area value of C1 (S_{BET} = 125 $m^2\ g^{-1}$) was two times larger than that of C2 (S_{BET} = 59 $m^2\ g^{-1}$), as confirmed by N_2 sorption analysis results. The specific surface areas of the Fe-N/C catalysts remained in the same order of magnitude (S_{BET} = 77–193 $m^2\ g^{-1}$), had developed nanofibers (HR-SEM), were successfully doped with Fe and N (SEM-EDX), and showed improved activity toward the ORR compared to carbon materials. Using C2, which had fewer impurities, instead of C1 as the carbon support did not enhance ORR activity, which may be due to its low specific surface area. After adding hydroxyapatite as an additional pore former to the Fe-N/C synthesis, N was not detected; instead, the catalysts contained phosphorus originating from HA. Fe and P compounds were formed in these materials (according to SEM-EDX and XRD). Therefore, the addition of HA did not improve the mesoporosity nor ORR activity of the catalyst. It was concluded that the choice and mass ratios of precursors as well as the pyrolysis temperature are important to optimize the physical and electrochemical characteristics of a Fe-N/C catalyst.

The most active catalyst, Fe-guan/C1-II-900, exhibited E_{onset} and $E_{1/2}$ values of 0.92 V vs RHE and 0.81 V vs RHE, respectively, and n = 4.0. These values are comparable to and even surpass other waste tire carbon based catalysts described in the literature, which shows that Fe-guan/C1-II-900 is a very good candidate for AEMFC single-cell measurements.

Acknowledgments

The author would like to express his utmost gratitude to PhD Rutha Jäger for supervising this thesis work. The author is grateful for her persistence, thoroughness in reviewing, and optimistic motivational messages throughout the author's studies.

The author would like to thank PhD Patrick Teppor for his practical guidance and for sharing his knowledge regarding synthesis methods.

The author also thanks BSc Annabel Raudsepp for synthesizing and providing the carbon material C2 as well as lending an ear to the author when the writing process did not quite go according to plan.

Additionally, the author thanks MSc Miriam Koppel and MSc Laura Kalder for help regarding N_2 sorption analyses, MSc Jaan Aruväli for XRD analyses, PhD Olga Volobujeva for HR-SEM and SEM-EDX analyses, MSc Karl-Ander Kasuk, PhD Peeter Valk, and PhD Jaak Nerut for advice and suggestions, and Professor Enn Lust.

This work was financially supported by the following sources:

- The Estonian Research Council (Proof-of-Concept Grant EAG273 and Personal Research Grant PRG676),
- The project "Increasing the knowledge intensity of Ida-Viru entrepreneurship" co-funded by the European Union (ÕÜF1), and
- The Estonian Ministry of Education and Research (Center of Excellence TK210 and TK141).

References

[1] "AR6 Synthesis Report: Climate Change 2023 — IPCC." https://www.ipcc.ch/report/sixth-assessment-report-cycle/ (accessed May 23, 2024).

[2] ERM, "The Fuel Cell Industry Review 2022".

[3] N. Ramaswamy and S. Mukerjee, "Alkaline Anion-Exchange Membrane Fuel Cells: Challenges in Electrocatalysis and Interfacial Charge Transfer," *Chem. Rev.*, no. 23, pp. 11945–11979, 2019.

[4] H. A. Firouzjaie and W. E. Mustain, "Catalytic Advantages, Challenges, and Priorities in Alkaline Membrane Fuel Cells," *ACS Catal.*, no. 1, pp. 225–234, 2020.

[5] J. Hyun and H.-T. Kim, "Powering the hydrogen future: current status and challenges of anion exchange membrane fuel cells," *Energy Environ. Sci.*, no. 12, pp. 5633–5662, 2023.

[6] J. Zhang, W. Zhu, T. Huang, C. Zheng, Y. Pei, G. Shen, Z. Nie, D. Xiao, Y. Yin, and M. D. Guiver, "Recent Insights on Catalyst Layers for Anion Exchange Membrane Fuel Cells," *Adv. Sci.*, no. 15, p. 2100284, 2021.

[7] Md. M. Hossen, Md. S. Hasan, Md. R. I. Sardar, J. bin Haider, Mottakin, K. Tammeveski, and P. Atanassov, "State-of-the-art and developmental trends in platinum group metal-free cathode catalyst for anion exchange membrane fuel cell (AEMFC)," *Appl. Catal. B Environ.*, p. 121733, 2023.

[8] F. Si, Y. Zhang, L. Yan, J. Zhu, M. Xiao, C. Liu, W. Xing, and J. Zhang, "4 - Electrochemical Oxygen Reduction Reaction," in *Rotating Electrode Methods and Oxygen Reduction Electrocatalysts*, W. Xing, G. Yin, and J. Zhang, Eds. Amsterdam: Elsevier, 2014, pp. 133–170.

[9] C. Li, Y. Wu, M. Fu, X. Zhao, S. Zhai, Y. Yan, L. Zhang, and X. Zhang, "Preparation of Fe/N Double Doped Carbon Nanotubes from Lignin in Pennisetum as Oxygen Reduction Reaction Electrocatalysts for Zinc–Air Batteries," *ACS Appl. Energy Mater.*, no. 4, pp. 4340–4350, 2022.

[10] G. Zuccante, M. Acciarri, C. L. Vecchio, I. Gatto, V. Baglio, N. Pianta, R. Ruffo, L. Navarini, and C. Santoro, "Oxygen reduction reaction platinum group metal-free electrocatalysts derived from spent coffee grounds," *Electrochimica Acta*, p. 144353, 2024.

[11] P. Teppor, R. Jäger, E. Härk, S. Sepp, M. Kook, O. Volobujeva, P. Paiste, Z. Kochovski, I. Tallo, and E. Lust, "Exploring Different Synthesis Parameters for the Preparation of Metal-Nitrogen-Carbon Type Oxygen Reduction Catalysts," *J. Electrochem. Soc.*, no. 5, p. 054513, 2020.

[12] R. Jäger, P. Teppor, M. Paalo, M. Härmas, A. Adamson, O. Volobujeva, E. Härk, Z. Kochovski, T. Romann, R. Härmas, J. Aruväli, A. Kikas, and E. Lust, "Synthesis and Characterization of Cobalt and Nitrogen Co-Doped Peat-Derived Carbon Catalysts for Oxygen Reduction in Acidic Media," *Catalysts*, no. 6, Art. no. 6, 2021.

[13] “Activated Carbon Market Size, Share & Trends Report, 2030.” https://www.grandviewresearch.com/industry-analysis/activated-carbon-market (accessed May 16, 2024).

[14] “New End-of-Life Tyres statistics for 2020 and 2021,” *ETRMA*. https://www.etrma.org/news/new-end-of-life-tyre-statistics-2020-2021/ (accessed May 23, 2024).

[15] J. D. Martínez, N. Puy, R. Murillo, T. García, M. V. Navarro, and A. M. Mastral, “Waste tyre pyrolysis – A review,” *Renew. Sustain. Energy Rev.*, pp. 179–213, 2013.

[16] L. Duval, G. Majeau-Bettez, F. Saunier, F. Maréchal, and M. Margni, “Optimization of the end-of-life tire repartition within the European treatment system to minimize its environmental impacts,” *J. Ind. Ecol.*, no. n/a.

[17] M. Kazemi, S. Parikhah Zarmehr, H. Yazdani, and E. Fini, “Review and Perspectives of End-of-Life Tires Applications for Fuel and Products,” *Energy Fuels*, no. 15, pp. 10758–10774, 2023.

[18] G. Bae, M. W. Chung, S. G. Ji, F. Jaouen, and C. H. Choi, “pH Effect on the H2O2-Induced Deactivation of Fe-N-C Catalysts,” *ACS Catal.*, no. 15, pp. 8485–8495, 2020.

[19] L. Osmieri, L. Pezzolato, and S. Specchia, “Recent trends on the application of PGM-free catalysts at the cathode of anion exchange membrane fuel cells,” *Curr. Opin. Electrochem.*, pp. 240–256, 2018.

[20] G. Reverdiau, A. Le Duigou, T. Alleau, T. Aribart, C. Dugast, and T. Priem, “Will there be enough platinum for a large deployment of fuel cell electric vehicles?,” *Int. J. Hydrog. Energy*, no. 79, pp. 39195–39207, 2021.

[21] A. E. Hughes, N. Haque, S. A. Northey, and S. Giddey, “Platinum Group Metals: A Review of Resources, Production and Usage with a Focus on Catalysts,” *Resources*, no. 9, Art. no. 9, 2021.

[22] K. Bloch, L. F. Johnson, M. Nkosi, and R. Ehrlich, “Precarious transition: a mortality study of South African ex-miners,” *BMC Public Health*, no. 1, p. 862, 2018.

[23] P. G. Santori, A. N. Mondal, D. R. Dekel, and F. Jaouen, “The critical importance of ionomers on the electrochemical activity of platinum and platinum-free catalysts for anion-exchange membrane fuel cells,” *Sustain. Energy Fuels*, no. 7, pp. 3300–3307, 2020.

[24] R. Gutru, Z. Turtayeva, F. Xu, G. Maranzana, R. Thimmappa, M. Mamlouk, A. Desforges, and B. Vigolo, “Recent progress in heteroatom doped carbon based electrocatalysts for oxygen reduction reaction in anion exchange membrane fuel cells,” *Int. J. Hydrog. Energy*, no. 9, pp. 3593–3631, 2023.

[25] C. Song and J. Zhang, “Electrocatalytic Oxygen Reduction Reaction,” in *PEM Fuel Cell Electrocatalysts and Catalyst Layers: Fundamentals and Applications*, J. Zhang, Ed. London: Springer, 2008, pp. 89–134.

[26] N. Ramaswamy and S. Mukerjee, “Influence of Inner- and Outer-Sphere Electron Transfer Mechanisms during Electrocatalysis of Oxygen Reduction in Alkaline Media,” *J. Phys. Chem. C*, no. 36, pp. 18015–18026, 2011.

[27] P. T. Williams, “Pyrolysis of waste tyres: A review,” *Waste Manag.*, no. 8, pp. 1714–1728, 2013.

[28] Q. Li, R. Cao, J. Cho, and G. Wu, “Nanocarbon Electrocatalysts for Oxygen Reduction in Alkaline Media for Advanced Energy Conversion and Storage,” *Adv. Energy Mater.*, no. 6, p. 1301415, 2014.

[29] M. Molina-Sabio and F. Rodríguez-Reinoso, “Role of chemical activation in the development of carbon porosity,” *Colloids Surf. Physicochem. Eng. Asp.*, no. 1, pp. 15–25, 2004.

[30] P. Teppor, R. Jäger, M. Koppel, O. Volobujeva, R. Palm, M. Månsson, E. Härk, Z. Kochovski, J. Aruväli, K. Kooser, S. Granroth, T. Käämbre, J. Nerut, and E. Lust, “Unlocking the porosity of Fe–N–C catalysts using hydroxyapatite as a hard template en route to eco-friendly high-performance AEMFCs,” *J. Power Sources*, p. 233816, 2024.

[31] S. Li, C. Cheng, X. Zhao, J. Schmidt, and A. Thomas, “Active Salt/Silica-Templated 2D Mesoporous FeCo-Nx-Carbon as Bifunctional Oxygen Electrodes for Zinc–Air Batteries,” *Angew. Chem. Int. Ed.*, no. 7, pp. 1856–1862, 2018.

[32] C. Moreno-Castilla, M. A. Ferro-Garcia, J. P. Joly, I. Bautista-Toledo, F. Carrasco-Marin, and J. Rivera-Utrilla, “Activated Carbon Surface Modifications by Nitric Acid, Hydrogen Peroxide, and Ammonium Peroxydisulfate Treatments,” *Langmuir*, no. 11, pp. 4386–4392, 1995.

[33] Y. Chen, J. Fitz Gerald, L. T. Chadderton, and L. Chaffron, “Nanoporous carbon produced by ball milling,” *Appl. Phys. Lett.*, no. 19, pp. 2782–2784, 1999.

[34] G. Long, K. Wan, M. Liu, X. Li, Z. Liang, and J. Piao, “Effect of pyrolysis conditions on nitrogen-doped ordered mesoporous carbon electrocatalysts,” *Chin. J. Catal.*, no. 8, pp. 1197–1204, 2015.

[35] F. Cataldo, “On the characterisation of carbon black from tire pyrolysis,” *Fuller. Nanotub. Carbon Nanostructures*, no. 5, pp. 368–376, 2020.

[36] D. Pantea, H. Darmstadt, S. Kaliaguine, and C. Roy, “Heat-treatment of carbon blacks obtained by pyrolysis of used tires. Effect on the surface chemistry, porosity and electrical conductivity,” *J. Anal. Appl. Pyrolysis*, no. 1, pp. 55–76, 2003.

[37] N. Muttil, S. Jagadeesan, A. Chanda, M. Duke, and S. K. Singh, “Production, Types, and Applications of Activated Carbon Derived from Waste Tyres: An Overview,” *Appl. Sci.*, no. 1, Art. no. 1, 2023.

[38] J. S. Gnanaraj, R. J. Lee, A. M. Levine, J. L. Wistrom, S. L. Wistrom, Y. Li, J. Li, K. Akato, A. K. Naskar, and M. P. Paranthaman, “Sustainable Waste Tire Derived Carbon Material as a Potential Anode for Lithium-Ion Batteries,” *Sustainability*, no. 8, Art. no. 8, 2018.

[39] M. Passaponti, L. Rosi, M. Savastano, W. Giurlani, H. A. Miller, A. Lavacchi, J. Filippi, G. Zangari, F. Vizza, and M. Innocenti, “Recycling of waste automobile tires: Transforming char in oxygen reduction reaction catalysts for alkaline fuel cells,” *J. Power Sources*, pp. 85–90, 2019.

[40] M. Passaponti, L. Lari, M. Bonechi, F. Bruni, W. Giurlani, G. Sciortino, L. Rosi, L. Fabbri, M. Vizza, V. K. Lazarov, C. Fontanesi, and M. Innocenti, “Optimisation Study of Co Deposition on Chars from MAP of Waste Tyres as Green Electrodes in ORR for Alkaline Fuel Cells,” *Energies*, no. 21, Art. no. 21, 2020.

[41] M. Muhyuddin, D. Testa, R. Lorenzi, G. M. Vanacore, F. Poli, F. Soavi, S. Specchia, W. Giurlani, M. Innocenti, L. Rosi, and C. Santoro, “Iron-based electrocatalysts derived from scrap tires for oxygen reduction reaction: Evolution of synthesis-structure-performance relationship in acidic, neutral and alkaline media,” *Electrochimica Acta*, p. 141254, 2022.

[42] G.-S. Kang, G. Lee, S. Y. Cho, H.-I. Joh, D. C. Lee, and S. Lee, “Recycling of waste tires by synthesizing N-doped carbon-based catalysts for oxygen reduction reaction,” *Appl. Surf. Sci.*, p. 149027, 2021.

[43] G. Lee, G.-S. Kang, J.-H. Jang, S. J. Yoo, H.-I. Joh, and S. Lee, “Upcycling waste tires to affordable catalysts for the oxygen reduction reaction,” *Int. J. Energy Res.*, no. 4, pp. 4645–4654, 2022.

[44] C. Du, Q. Tan, G. Yin, and J. Zhang, “5 - Rotating Disk Electrode Method,” in *Rotating Electrode Methods and Oxygen Reduction Electrocatalysts*, W. Xing, G. Yin, and J. Zhang, Eds. Amsterdam: Elsevier, 2014, pp. 171–198.

[45] R. E. Davis, G. L. Horvath, and C. W. Tobias, “The solubility and diffusion coefficient of oxygen in potassium hydroxide solutions,” *Electrochimica Acta*, no. 3, pp. 287–297, 1967.

[46] C. Du, Y. Sun, T. Shen, G. Yin, and J. Zhang, “7 - Applications of RDE and RRDE Methods in Oxygen Reduction Reaction,” in *Rotating Electrode Methods and Oxygen Reduction Electrocatalysts*, W. Xing, G. Yin, and J. Zhang, Eds. Amsterdam: Elsevier, 2014, pp. 231–277.

[47] R. Bardestani, G. S. Patience, and S. Kaliaguine, “Experimental methods in chemical engineering: specific surface area and pore size distribution measurements—BET, BJH, and DFT,” *Can. J. Chem. Eng.*, no. 11, pp. 2781–2791, 2019.

[48] P. E. J. Flewitt and R. K. Wild, *Physical methods for materials characterisation*, 2nd ed. Bristol ; Philadelphia: Institute of Physics Pub, 2003.

[49] A. A. Bunaciu, E. gabriela Udriştioiu, and H. Y. Aboul-Enein, “X-Ray Diffraction: Instrumentation and Applications,” *Crit. Rev. Anal. Chem.*, no. 4, pp. 289–299, 2015.

[50] A. Malaika, J. Kowalska-Kuś, K. Końska, K. Ptaszyńska, A. Jankowska, A. Held, K. Wróblewski, and M. Kozłowski, “Upgrading Pyrolytic Residue from End-of-Life Tires to Efficient Heterogeneous Catalysts for the Conversion of Glycerol to Acetins,” *Molecules*, no. 24, Art. no. 24, 2023.

[51] W. D. Nicoll and A. F. Smith, “Stability of Dilute Alkaline Solutions of Hydrogen Peroxide,” *Ind. Eng. Chem.*, no. 12, pp. 2548–2554, 1955.

[52] A. Raudsepp, R. Jäger, J. Nerut, P. Valk, P. Teppor, M. Koppel, J. Aruväli, J. Laanemäe, W. Lobjakas, and E. Lust, “Preparation of Membrane Electrode Assemblies Using Waste Tire Derived Carbon Supported Platinum Catalyst,” *ECS Trans.*, no. 5, p. 51, 2023.

[53] J. A. Conesa, I. Martín-Gullón, R. Font, and J. Jauhiainen, “Complete Study of the Pyrolysis and Gasification of Scrap Tires in a Pilot Plant Reactor,” *Environ. Sci. Technol.*, no. 11, pp. 3189–3194, 2004.

[54] S. Ratso, I. Kruusenberg, M. Käärik, M. Kook, R. Saar, P. Kanninen, T. Kallio, J. Leis, and K. Tammeveski, “Transition metal-nitrogen co-doped carbide-derived carbon catalysts for oxygen reduction reaction in alkaline direct methanol fuel cell,” *Appl. Catal. B Environ.*, pp. 276–286, 2017.

[55] G. Ćirić-Marjanović, I. Pašti, and S. Mentus, “One-dimensional nitrogen-containing carbon nanostructures,” *Prog. Mater. Sci.*, pp. 61–182, 2015.

[56] J. Laanemäe, R. Jäger, P. Teppor, O. Volobujeva, and E. Lust, “Waste Tire Derived Carbon Support for Non-Platinum-Group Metal Catalyst Materials for Oxygen Reduction Reaction in Alkaline Medium,” *ECS Trans.*, no. 5, p. 63, 2023.

[57] H. Zhang, S. Hwang, M. Wang, Z. Feng, S. Karakalos, L. Luo, Z. Qiao, X. Xie, C. Wang, D. Su, Y. Shao, and G. Wu, “Single Atomic Iron Catalysts for Oxygen Reduction in Acidic Media: Particle Size Control and Thermal Activation,” *J. Am. Chem. Soc.*, no. 40, pp. 14143–14149, 2017.

[58] Y. Huang, Y. Chen, M. Xu, T. Asset, P. Tieu, A. Gili, D. Kulkarni, V. De Andrade, F. De Carlo, H. S. Barnard, A. Doran, D. Y. Parkinson, X. Pan, P. Atanassov, and I. V. Zenyuk, “Catalysts by pyrolysis: Direct observation of chemical and morphological transformations leading to transition metal-nitrogen-carbon materials,” *Mater. Today*, pp. 53–68, 2021.

[59] M. Barczak, Y. Elsayed, J. Jagiello, and T. J. Bandosz, “Exploring the effect of ultramicropore distribution on gravimetric capacitance of nanoporous carbons,” *Electrochimica Acta*, pp. 236–247, 2018.

[60] N. Norouzi, F. A. Choudhury, and H. M. El-Kaderi, “Iron Phosphide Doped, Porous Carbon as an Efficient Electrocatalyst for Oxygen Reduction Reaction,” *ACS Appl. Energy Mater.*, no. 3, pp. 2537–2546, 2020.

[61] K. P. Singh, E. J. Bae, and J.-S. Yu, “Fe–P: A New Class of Electroactive Catalyst for Oxygen Reduction Reaction,” *J. Am. Chem. Soc.*, no. 9, pp. 3165–3168, 2015.

[62] D. P. Leonard, W. F. Stickle, and X. Ji, “Carbon-Supported Iron Phosphides: Highest Intrinsic Oxygen Evolution Activity of the Iron Triad,” *ACS Appl. Energy Mater.*, no. 8, pp. 3593–3597, 2018.

Non-exclusive licence to reproduce the thesis and make the thesis public

I, Joel Indrek Martin Laanemäe,

1. grant the University of Tartu a free permit (non-exclusive licence) to reproduce, for the purpose of preservation, including for adding to the DSpace digital archives until the expiry of the term of copyright, my thesis "Fe-N/C Catalysts Based on Carbon Derived from Waste Tires: Advancing Oxygen Reduction Reaction in Alkaline Solution" supervised by Rutha Jäger, PhD

2. I grant the University of Tartu a permit to make the thesis specified in point 1 available to the public via the web environment of the University of Tartu, including via the DSpace digital archives, under the Creative Commons licence CC BY NC ND 4.0, which allows, by giving appropriate credit to the author, to reproduce, distribute the work and communicate it to the public, and prohibits the creation of derivative works and any commercial use of the work until the expiry of the term of copyright.

3. I am aware of the fact that the author retains the rights specified in points 1 and 2.

4. I confirm that granting the non-exclusive licence does not infringe other persons' intellectual property rights or rights arising from the personal data protection legislation.

/*Signed digitally*/

Joel Indrek Martin Laanemäe

30.05.2024